Макрогетероциклы
http://mhc-isuct.ru

DOI: 10.6060/mhc235113p

Molecular Structure and Vibrational Spectra of 4-(4-Hydroxyphenylazo)phthalonitrile: DFT Study

Alexander E. Pogonin,[@] Ivan Yu. Kurochkin, Alyona S. Malyasova, Ksenia V. Ksenofontova, and Oskar I. Koifman

Ivanovo State University of Chemistry and Technology, 153000 Ivanovo, Russian Federation
[@]E-mail: pogonin@isuct.ru

Dedicated to Academician of the Russian Academy of Sciences Irina P. Beletskaya on the occasion of her Anniversary

Structural features, conformational manifold and isomeric forms of 4-(4-hydroxyphenylazo)phthalonitrile (p-HPhAPN) were studied by DFT calculations (B3LYP) using QTAIM, NPA, NBO, NCI, SAPT0 analysis. The influence of hydroxyl and nitrile groups on the geometric structure of the molecule was analyzed in comparison with the initial azobenzene and isomers differing in the location of the hydroxyl group – m-HPhAPN, o-HPhAPN. For the initial p-HPhAPN, 8 possible models were considered, for isomeres o-HPhAPN and m-HPhAPN – 32 and 16 models, respectively. The variety of the chosen models is due to the possibility of (a) different arrangement of hydrogen atoms of the hydroxyl group, determined by the corresponding torsion angle, (b) cisoid/transoid arrangement of nitrile groups with respect to the azo group, (c) cisoid/transoid arrangement of the hydroxyl group with respect to the azo group, (d) tautomerism, and (e) cis-trans isomerism. Assignment of vibrational modes of p-HPhAPN was carried out via potential energy distribution (PED) analysis among internal coordinates. The PED of most normal vibrations for p-HPhAPN, as well as for initial azobenzene, has a complex character. Changes in the IR spectra caused by the considered structural changes are noted.

Keywords: Phthalonitriles, azo dyes, molecular structure, vibrational spectra, quantum chemical calculation, normal mode.

Молекулярная структура и колебательные спектры 4-(4-гидроксифенилазо)фталонитрила: DFT изучение

А. Е. Погонин,[@] И. Ю. Курочкин, А. С. Малясова, К. В. Ксенофонтова, О. И. Койфман

Ивановский государственный химико-технологический университет, 153000 Иваново, Российская Федерация
[@]E-mail: pogonin@isuct.ru

Посвящается Академику Российской академии наук Ирине Петровне Белецкой в связи с ее юбилеем

С помощью квантово-химических расчетов (метод теории функционала плотности, функционал B3LYP) и проведенных QTAIM (квантовая теория атомов в молекуле), NPA (анализ заселенности натуральных атомных орбиталей), NBO (натуральные орбитали связей), NCI (анализ нековалентных взаимодействий), SAPT0 (адаптированная по симметрии теория возмущений) анализов изучены особенности строения, конформационного многообразия и изомерных форм 4-(4-гидроксифенилазо)фталонитрила (p-HPhAPN). Выполнен анализ влияния гидроксильной и нитрильных групп на геометрическое строение молекулы в сравнении с исходным азобензолом (Ab) и изомерами, отличающимися расположением гидроксильной группы, – m-HPhAPN, o-HPhAPN. В ходе исследования рассмотрено 8 возможных структур для исходной молекулы p-HPhAPN, а для его изомерных форм o-HPhAPN и m-HPhAPN – 32 и 16 структур, соответственно. Многообразие выбранных моделей обусловлено возможностью (а) различного расположения атомов водорода

гидроксильной группы, определяемого соответствующим торсионным углом, (б) цисоидного/трансоидного расположения нитрильных групп по отношению к азогруппе, (в) цисоидного/трансоидного расположения гидроксильной группы по отношению к азогруппе, (г) таутомерии и (д) цис-транс-изомерии. Проведено описание колебаний p-HPhAPN на основе анализа распределения потенциальной энергии (РПЭ) форм нормальных колебаний по естественным колебательным координатам. РПЭ большинства нормальных колебаний по внутренним координатам для p-HPhAPN, как и для Ab, имеет сложный характер. Выполнен анализ влияния геометрического строения рассмотренных структур на соответствующие ИК-спектры.

Ключевые слова Фталонитрилы, азокрасители, молекулярная структура, колебательные спектры, квантовая химия, нормальные колебания.

Introduction

Azo compounds R_1-N=N-R_2 and especially azobenzenes are considered as promising compounds for the design of functional and "smart" materials.[1,2] Photoisomerization (*trans* ⇄ *cis* or *E*- ⇄ *Z*-) is one of the most interesting properties of azo dyes which makes these compounds suitable for use in a wide range of applications, such as the development of various sensors, molecular switches, optical data storage, non-linear optics, color-changing materials, *etc*.[3–8] Some representatives of azo dyes based on phtalonitriles can additionally be considered as precursors for the synthesis of phthalocyanines with extended light absorption range.[9] This interest is due to the idea that narrowness of the absorption band of phthalocyanines can be resolved by introduction of a unit with its own chromophore system to macrocyclic core. These substances containing macrocycle and azo chromophores are promising for photodynamic cancer therapy.[9]

Due to the great practical importance of azo dyes, their structural features must be studied to interpret and predict chemical, physical and biological properties. Structural studies usually include both experimental (X-ray diffraction, gas electron diffraction (GED), *etc*.) and theoretical (molecular dynamics and quantum chemical (QC) calculations) methods. The structure of several azo dyes, in particular the structure of parent azobenzene (**Ab**), was investigated by both experimental methods mentioned above.[10–18] QC calculations are used to interpret the obtained experimental characteristics and predict the properties of substances. Moreover, molecular modeling is often used for reasonable and efficient design of new functional azo compounds, for example for applying in dye sensitized solar cells.[19,20]

In this paper, we investigated the structures, vibrational spectra, conformational and isomeric diversity of 4-(4-hydroxyphenylazo)phthalonitrile (**p-HPhAPN**) using density functional theory (DFT) calculations. To study the effect of cyano and hydroxyl substituents on the structure and properties, the molecules of 4,4'-dihydroxyazobenzene (**Ab-2OH**) and 3,3',4,4'-tetracyanoazobenzene (**Ab-4CN**) were also calculated (Figure 1).

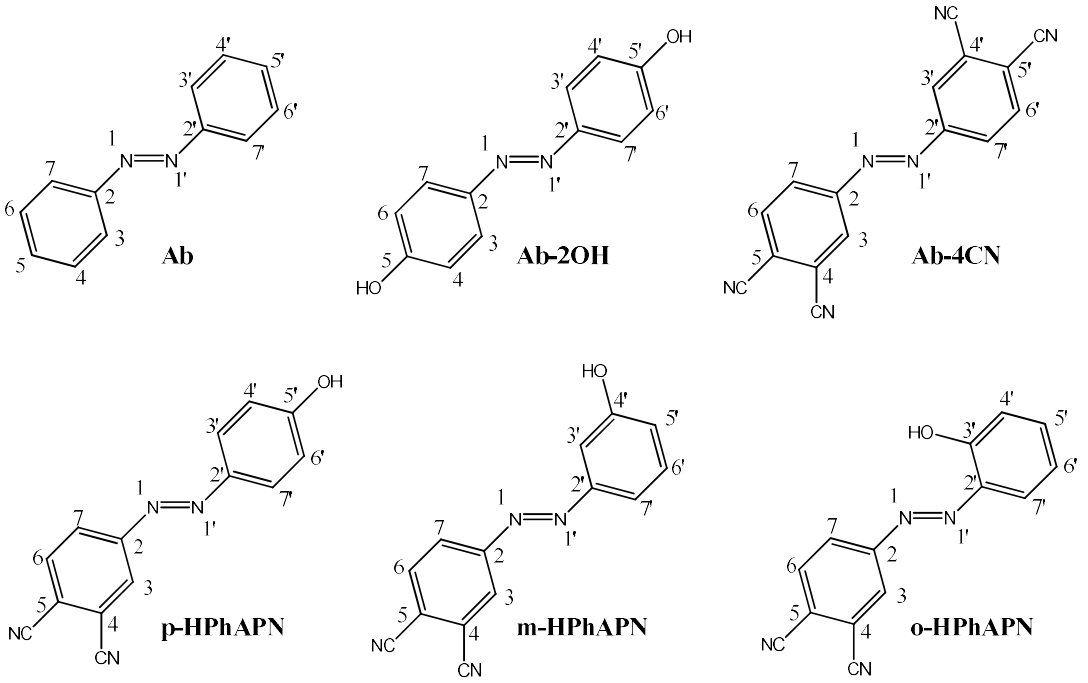

Figure 1. Structures of the investigated molecules and atom labeling scheme used throughout a paper: **Ab** – azobenzene; **Ab-2OH** – 4,4'-dihydroxyazobenzene; **Ab-4CN** – 3,3',4,4'-tetracyanoazobenzene; **p-HPhAPN** – 4-(4-hydroxyphenylazo)phthalonitrile, 4-[(4-hydroxyphenyl)diazenyl]benzene-1,2-dicarbonitrile; **m-HPhAPN** – 4-(3-hydroxyphenylazo)phthalonitrile; 4-[(3-hydroxyphenyl)diazenyl]benzene-1,2-dicarbonitrile; **o-HPhAPN** – 4-(2-hydroxyphenylazo)phthalonitrile, 4-[(2-hydroxyphenyl)diazenyl]benzene-1,2-dicarbonitrile. Substance names follow IUPAC recommendations, not the labeling scheme used.

Experimental

Calculation details

QC calculations were performed using the Gaussian 09 program[21] in the framework of density functional theory (DFT) method. Optimized geometries and all of the harmonic vibrational frequencies were obtained using B3LYP functional with 6-31++G** basis set[22–25] for all atoms. The basis set was taken from Basis Set Exchange software.[26–28] All optimized structures from QC calculations are given in *Supplementary materials*. The natural bond orbital analysis was performed as it is implemented in NBO 5.0 program.[29] QTAIM (Quantum theory of atoms in molecules) analysis was performed using AIMAll software package.[30] For hydrogen bonds the presence of critical point (3,-1) is a necessary and sufficient condition – the values of electron density distribution function ρ(r) and Laplacian of electron density $\nabla^2\rho(r)$ in bond critical points (BCPs) should lie in the range from 0.002 to 0.035 a.u. and from 0.024 to 0.139 a.u., respectively.[31] For estimation of non-covalent interactions between –Ph-OH and –Ph-2CN subunits non-covalent interactions index (NCI) and functional group intramolecular symmetry-adapted perturbation theory (F/I-SAPT0)[32–34] calculations were performed. NCI[35] allowed to visualize the areas of weak interactions for the reduced density gradient (RDG) value = 0.6. For this purpose, it was used open-source Multiwfn software.[36] F/I-SAPT0/6-31++G** method (realized in the PSI4 program[37]) is used to measure these interactions quantitatively and to divide these forces in more details according to their physical meaning.

The assignments of vibrational modes of **p-HPhAPN** and **Ab** were carried out by the PED analysis among internal coordinates using the VibModule program.[38] In the course of the analysis, the works[39–46] devoted to parent compounds and analogues were taken into account. Visualization of vibrations is realized by the ChemCraft software.[47]

General

The synthesis was carried out in accordance with the procedure described in the article.[48] Infrared (IR) spectra were obtained by means of a Shimadzu IRAffinity-1 Fourier transform IR spectrophotometer equipped with a Specac Quest ATR Diamond GS10800-B accessory in the attenuated total reflectance mode.

Results and Discussion

Molecular structure of initial azobenzenes

Initial **E-Ab** has a planar structure of the C_{2h} symmetry,[44,49–52] which was confirmed by GED.[18] The planar structure is supported by the presence of π-system delocalization.[53] It is confirmed by strong donor-acceptor interactions between bonding $\pi(C_2\text{-}C_3)$ natural orbitals and the antibonding $\pi^*(N_1\text{-}N'_1)$.[53] The presence of a large delocalized π-system is also indicated by the values of Wiberg bond indexes (WI) obtained by natural atomic orbital analysis: for **E-Ab** $WI(N_1\text{-}N'_1)=1.76$ and $WI(N_1\text{-}C_2)=1.11$, whereas analogues values for diazene and methylamine were 2.07 and 1.02. Transition **E-Ab→Z-Ab** leads to an weakening of interaction between nitrogen atoms and phenyl groups and significantly affects geometric parameters of the azo bridge: $r_e(N_1\text{-}N'_1)$ decreases by 0.009 Å, $r_e(N_1\text{-}C_2)$ increases by 0.017 Å. Z-isomer is characterized by a folded structure in which the planes of phenyl rings do not lie "face to face"[54] and are twisted relative to each other. This twist can be explained by energy balance between orbital conjugation of the phenyl rings and azo bridge on the one hand and steric repulsion of the neighboring phenyl groups on the other hand, by analogy with the situations described in [55,56]. According to our calculations the energy gain of the **E-Ab** structure is 66.1 kJ·mol^{-1} as compared to the U-shaped structure (C_2 symmetry) of **Z-Ab**.

Substitution effects

Introduction of cyano and hydroxyl substituents (**Ab→Ab-2OH**, **Ab-4CN**) leads to shortening of NC internuclear distances. The interaction between the bridge and phenyl rings in **E-Ab-4CN** and **E-Ab** are approximately the same. But for **E-Ab-2OH** this interaction becomes more pronounced. This is confirmed by the results of the NBO analysis, as well as by the values of the calculated rotation barriers of corresponding phenyl rings around the bond $N_1\text{-}N'_1$. In the case of **E-Ab**, this value is 25.2 kJ·mol^{-1}. Rotation barriers of rings substituted by -CN groups are in a small range (~22-25 kJ·mol^{-1}) for different considered molecules. For rings substituted by -OH group, rotation barrier increases in the series **E-Ab-2OH** (31.3 kJ·mol^{-1}), **E-m-HPhAPN** (31.8 kJ·mol^{-1}), **E-p-HPhAPN** (40.7 kJ·mol^{-1}), **E-o-HPhAPN** (>67 kJ·mol^{-1}). In the case of asymmetric molecules **HPhAPN**, the interaction between the azo bridge and -Ph-OH moiety is stronger than the corresponding interaction with -Ph-2CN moiety. Distances $r_e(N'_1\text{-}C'_2)$ in **HPhAPN** molecules are shorter than distances $r_e(N_1\text{-}C_2)$ and the distances $r_e(N'_1\text{-}C'_2)$ elongate to a greater extent during E-→Z- isomerization. The substitution of hydrogen atoms by a -CN and -OH groups in positions C_4 and C_5 does not lead to significant changes in energy differences between E- and Z-isomers compared to the initial **Ab** (66.1 kJ·mol^{-1} for **Ab**, ~70 kJ·mol^{-1} for **p-HPhAPN** and **m-HPhAPN**). In the case of **o-HPhAPN** this energy difference increases due to the presence of intramolecular interactions, which are described below.

Upon **E-p-HPhAPN→E-o-HPhAPN** transition the $N_1\text{-}N'_1$ distance increases by 0.012 Å, $N_1\text{-}C_2$, $N'_1\text{-}C'_2$ and C-O shortens by 0.018, 0.004, 0.022 Å, respectively (Table 1). In the case of **E-p-HPhAPN→E-m-HPhAPN** transition the changes in the geometric parameters are weaker: the elongation of $N_1\text{-}C_2$ and C-O distances by 0.009 Å and 0.006 Å are the most noticeable. The C-C bond lengths in the -Ph-OH fragment also undergo considerable changes: up to 0.018 Å for some distances at the **E-p-HPhAPN→ E-o-HPhAPN** transition and up to 0.007 Å **E-p-HPhAPN→ E-m-HPhAPN**.

*Isomerism and conformational diversity of **HPhAPN***

The asymmetrical introduction of cyano and hydroxyl substituents (**E-Ab→E-HPhAPN**) increases the conformational diversity. Conformational multiformity of **p-HPhAPN** and **m-HPhAPN** is associated with the possible rotation of phenyl and hydroxyl groups around the N-C and O-H bonds, respectively. Rotation barriers of hydroxyl group increases in a similar way as in the case of the rotation of Ph-OH moiety – from 17.3 kJ·mol^{-1} for **E-Ab-2OH** to >65.9 kJ·mol^{-1} for **E-o-HPhAPN**. Possible cisoid and transoid conformers of **E-p-HPhAPN** differ in the arrangements of cyano group and hydrogen atom of hydroxyl group with respect to the azo bridge. The naming principle is based on the locations of the group or atom

relative to the chain $C_5\cdots N_1\text{-}N'_1\cdots C'_5$: for –CN groups – cisoid (*a* and *b* models) and transoid (*c* and *d* models) arrangements; for H – cisoid (*b* and *d* models) and transoid (*a* and *c* models) arrangements (Figure 2). Considering the Z-isomers, there are four more possible structures. According to QC calculations, the energy differences between models differing by arrangement of –CN groups do not exceed 1 kJ·mol^{-1}. For H atom of –OH group arrangements, corresponding differences do not exceed 3 kJ·mol^{-1}. The number of possible structures of **m-HPhAPN** is increased by possibility of cisoid and transoid arrangements of -OH group (*a, b, c, d* and *e, f, g, h*, respectively, Figure 3, S1).

In the case of **o-HPhAPN** conformational analysis is additionally complicated by the appearance of tautomerism: hydrogen atom can form a hydrogen bond with a bridging nitrogen atom and even migrate to it to form a keto- structure. Enol- structure *b* possesses the lowest energy (Figure 3). The structure is characterized by the intramolecular strong hydrogen bond formation (according to QTAIM analysis, the values of ρ(r) in BCP($N_1\cdots H$) is 0.052 a.u., the value of $\nabla^2\rho(r)$ is 0.125 a.u.). Model *f* is a less energetically preferable structure. It is characterized by an intramolecular hydrogen bond (ρ(r) is 0.021 a.u., the value of $\nabla^2\rho(r)$ is 0.074 a.u.) formed by the H atom of the hydroxyl group and the neighbor nitrogen atom N'_1. Considering the factor of the possible arrangements of the cyano groups relative to the azo bridge, transoid and cisoid conformers differ slightly (by no more than 3 kJ·mol^{-1}). It is worth noting disturbing the planarity of the structures *f, h, m, n, o, p* caused by the rotation of the –Ph-2CN moiety. This fact can be explained by steric repulsions between hydrogen atoms.

Table 1. Selected structural parameters of conformers and isomers of the HPhAPN obtained by B3LYP calculations.

	Ab		**p-HPhAPN**		**o-HPhAPN**				**m-HPhAPN**	
	E-	Z-	E-	Z-	E-		Z-		E-	Z-
			a	*za*	*b*	*i*	*zf*	*zb*	*b*	*za*
ΔE, kJ·mol^{-1}	0.0	66.1	0.0	70.5	*0.0*	13.5	79.8	106.4	*0.5*	68.2
$r_e(N_1\text{-}N'_1)$, Å	1.258	1.249	1.262	1.251	*1.274*	1.310	1.254	1.253	*1.259*	1.248
$r_e(N'_1\text{-}C'_2)$, Å	1.420	1.436	1.404	1.424	*1.386*	1.333	1.410	1.434	*1.413*	1.434
$r_e(N_1\text{-}C_2)$, Å	1.420	1.436	1.418	1.428	*1.414*	1.395	1.425	1.433	*1.420*	1.433
$\alpha_e(N_1\text{-}N'_1\text{-}C'_2)$, °	115.3	124.0	116.0	124.7	*116.9*	118.2	127.9	123.1	*115.7*	123.7
$\alpha_e(N'_1\text{-}N_1\text{-}C_2)$, °	115.3	124.0	114.5	125.0	*115.5*	121.0	124.8	124.1	*114.5*	124.3
$\chi_e(C'_2\text{-}N'_1\text{-}N_1\text{-}C_2)$, °	180.0	9.6	180.0	10.8	*180.0*	180.0	9.6	9.3	*180.0*	9.6
$\chi_e(N_1\text{-}N'_1\text{-}C'_2\text{-}C'_3)$, °	0.0	50.7	180.0	35.6	*0.0*	0.0	22.0	57.4	*0*	48.0
$\chi_e(N'_1\text{-}N_1\text{-}C_2\text{-}C_3)$, °	0.0	50.7	0.0	58.6	*0.0*	0.0	63.8	48.6	*0*	55.0
r_e(C-O), Å	-	-	1.361	1.361	*1.339*	1.262	1.347	1.367	*1.367*	1.367
$r_e(C'\text{-}C')_{average}$, Å	1.400	1.399	1.400	1.400	*1.405*	1.423	1.404	1.400	*1.400*	1.399
$r_e(C\text{-}C)_{average}$, Å	1.400	1.399	1.403	1.403	*1.403*	1.403	1.403	1.403	1.403	1.403

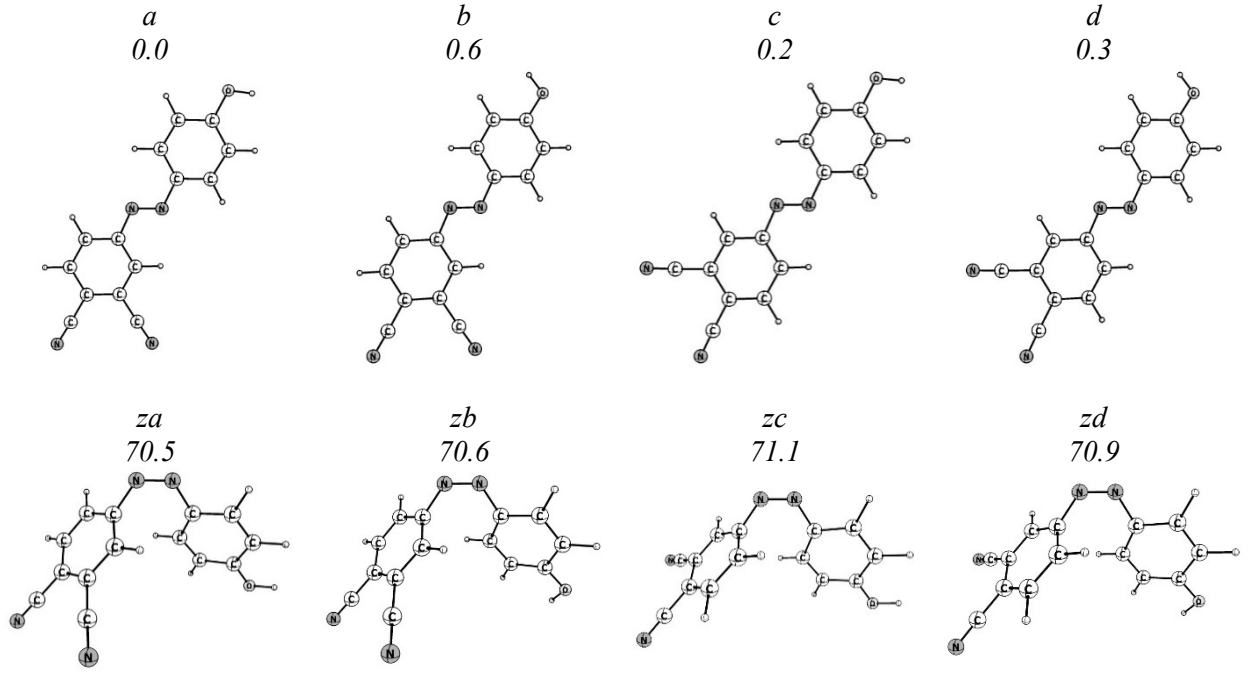

Figure 2. Conformer and isomer models of **p-HPhAPN** and appropriate relative energies (kJ·mol^{-1}).

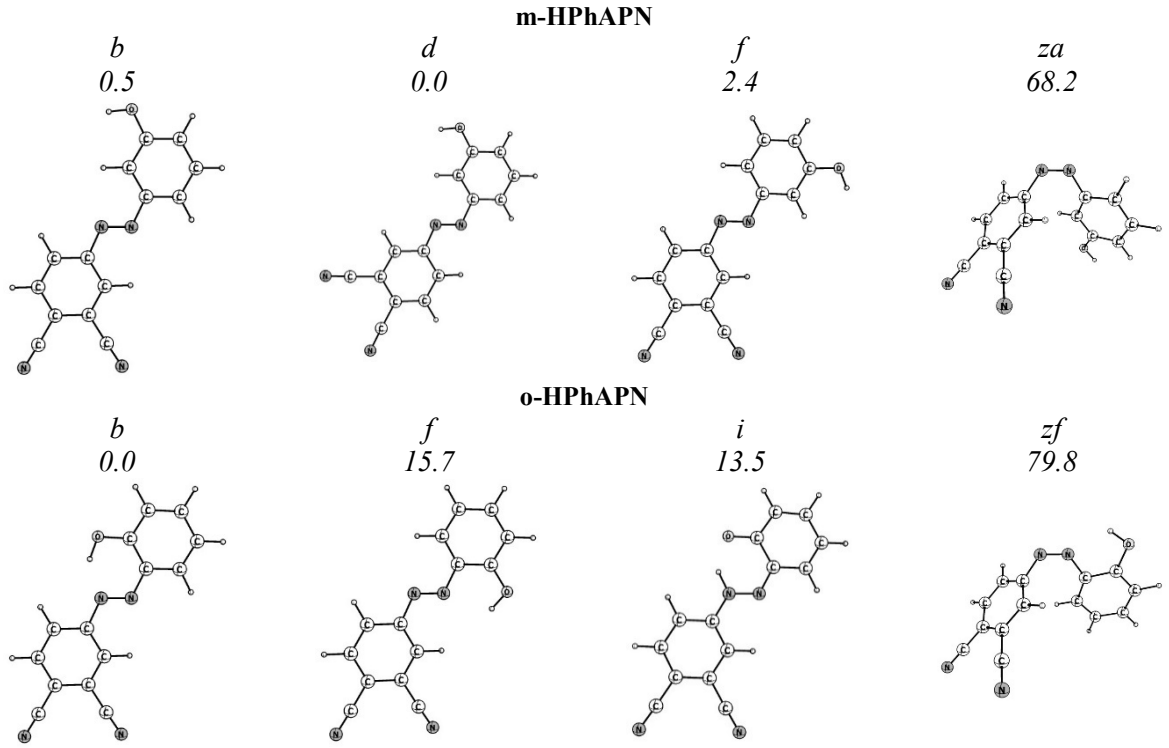

Figure 3. Several conformer and isomer models of **m-HPhAPN** and **o-HPhAPN** and appropriate relative energies (kJ·mol^{-1}). A complete set of considered structures is presented in Figure S1-S3.

Table 2. Second order perturbation energies $E^{(2)}$ (kcal·mol^{-1}) of donor-acceptor interactions between azo bridge and phenyl fragments for **Ab** and p-**HPhAPN**.

$E^{(2)}$	**Ab**				**p-HPhAPN**			
	E-		Z-		E- *a*		Z- *za*	
	N-N ⇄ C-C							
	all [a]	π→π* [b]	all [a]	π→π* [b]	all [a]	π→π* [b]	all [a]	π→π* [b]
Total [c]	67.8	60.7	42.7	25.6	71.9	64.2	42.8	25.4
-Ph' (-Ph-OH) [d]	33.9	30.4	21.4	12.8	38.9	34.9	30.1	25.4
-Ph (-Ph-2CN) [e]	33.9	30.4	21.4	12.8	32.9	29.4	12.7	0.0
	C-N ⇄ C-C							
Total [c]	22.3	0.0	23.8	0.0	21.3	0.0	22.0	0.0
-Ph' (-Ph-OH) [f]	11.2	0.0	11.9	0.0	10.7	0.0	11.2	0.0
-Ph (-Ph-2CN) [g]	11.2	0.0	11.9	0.0	10.6	0.0	10.8	0.0
	C-N ⇄ C-N							
Total	8.4	0.0	0.0	0.0	8.0	0.0	0.5	0.0

[a] $E^{(2)}$ contains π→π*, π→σ*, σ→π*, σ→σ* interactions;
[b] $E^{(2)}$ contains only π→π* interactions;
[c] The total energies $E^{(2)}$ are divided into two components related to interactions between azo bridge and different subunits: for **p-HPhAPN** there are -Ph-OH and -Ph-2CN.
[d] $E^{(2)}$ contains interactions between NBO(N'_1-N_1) and NBO(C'_2-C'_3);
[e] $E^{(2)}$ contains interactions between NBO(N'_1-N_1) and NBO(C_2-C_3);
[f] $E^{(2)}$ contains interactions between NBO(N'_1-C'_2) and NBO(C'_3-C'_4);
[g] $E^{(2)}$ contains interactions between NBO(N_1-C_2) and NBO(C_3-C_4).

According to QC calculations, the energy difference between *enol*-form *b* and *keto*-form *i* structures is ~14 kJ·mol^{-1}. Hydrogen atom migration from the hydroxyl group to nitrogen atom strongly affects the structure and electron density distribution of azo bridge and -Ph=O moiety (Table 1). Upon *b*→*i* transition, the NICS(0) and NICS(1) indexes, calculated in the center and 1 Å above the center of the -Ph-OH fragments, changes from -6.9 and -7.9 to 0.1 and -3.3, respectively (Table S1). *Keto*-form *i* is also characterized by the presence of a hydrogen bond (according to QTAIM analysis, the values of ρ(r) in BCP(O···H) is 0.055 a.u., the value of $\nabla^2\rho(r)$ is 0.161 a.u.).

NBO analysis

The above structural features of **HPhAPN** isomeric forms are closely related to their electronic structure. The

transition E-⟶Z- results in the destruction of the broad π-delocalized system. The sum energies of the donor-acceptor interactions $E^{(2)}$ for the σ and π natural orbitals of the N-N and C-N bonds with the antibonding C-C of the adjacent subunits are listed in the Table 2. The orbital interactions N-N with C-C in E-isomer are significantly stronger than in Z-isomer. The contribution π(N-N)⟶π*(C-C) interaction types are prevail in the $E^{(2)}$ value. The functionalization by -CN and -OH substituents leads to some asymmetry in the values of stabilization energy $E^{(2)}$ associated with interactions between the azo-bridge and different aryl moieties. Obtained data show that in **Z-p-HPhAPN** molecule -Ph-2CN subunit does not actually participate in the π-overlap with N-N orbitals. This is also confirmed by the fact that rotation angle of -Ph-2CN moiety χ(N'_1-N_1-C_2-C_3)=58.6 ˚ is bigger than appropriate one for -Ph-OH subunit χ(N_1-N'_1-C'_2-C'_3)=35.6 ˚. Noticeable that the E-⟶Z-transition is accompanied by a decrease in the $E^{(2)}$ energy, and the σ⟶σ*, σ⟶π* types begin to have a greater contribution in N-N⇄C-C orbital interactions. The energy of orbital interactions N-C⇄C-C are approximately similar for E- and Z-isomers.

Table 3 summarizes the most prominent energies of the nitrogen lone pair LP(N) with all orbitals encountered and sorted by bond types (C-C, C-N, O-H). In E-structures the most noticeable interactions of LP(N) are with the σ*(C-C). The Z- isomers are characterized by additional interactions LP(N)⟶σ*(N-C) with stabilization energy over 10 kcal·mol^{-1}. Thus, the stabilization of the Z- structure is largely due to the interactions of electron nitrogen pairs.[53]

The nature of interactions between LP(N) and periphery is highly different in E- and Z- structures. The composition of atomic orbitals (AO) forming the hybrid orbital (HO) for nitrogen atoms changes. While in the E-structures LP(N, N') were hybridized by sp^2 type, in Z-isomers LP(N') is composed by p AO. As a result, there is interaction of the type LP(N')⟶π*(C-C) with the value $E^{(2)}$=28.4 kcal·mol^{-1} in the case of the **Z-p-HPhAPN**.

For E-isomers, the introduction of -OH and -CN groups into the molecule does not have a clear effect on the interactions between LP(N'_1) and antibonding C-N, C-C orbitals. However, in the case of **E-o-HPhAPN** (model *b*, Figure 3) there is a hydrogen bond between one of the nitrogen atoms and -OH group. In NBO terms, the presence of this bond is identified as a high energy interaction of the LP(N)⟶σ*(O-H) type with $E^{(2)}$=32.3 kcal·mol^{-1}. For **Z-p-HPhAPN**, interactions between LP(N'_1) and antibonding C-C orbitals are more intense than for parent **Z-Ab**.

The migration of the H atom to one of the nitrogen atoms strongly affects the redistribution of the electron density of **E-o-HPhAPN** molecule. In the keto structures, strong π⟶π* interactions between the C-C and C-N orbitals are detected and π⟶π* interactions between the C-C and N-N orbitals are not detected in contrast to the enolic structure. This leads to a strong shortening of the C-N bonds and elongation of the N-N bonds in the keto structures, as compared to the enol ones.

In the **E-o-HPhAPN** structure *i*, one of the LP(N) is located on the p orbital as it was in **E-p-HPhAPN** (model *za*). It leads to an increase in the value of the total energy $E^{(2)}$, which includes all interactions of LP(N). In the case of the keto-structure the total $E^{(2)}$ is higher than in **Z-p-HPhAPN** (model *za*).

NCI analysis

One of the factors affecting the stabilization of one or another isomeric structure can be weak noncovalent interactions. In the NCI method, the electron density gradient ρ(r) used in AIM is recalculated into the so-called reduced density gradient (dimensionless) (RDG - reduced density gradient). The RDG can be plotted on an isosurface, thus mapping areas of weak interactions. NCI allows to partial identify non-covalent interactions by their types. One can distinguish areas of steric repulsion (red); areas indicating the presence of hydrogen bonds (blue); areas of Van der Waals interactions (green). In Figure 4 the red areas in the centers of the phenyl rings corresponding to the steric repulsion are clearly visible. The remaining detected areas are related to the different types of van der Waals interactions (mostly green) or mixed-type interactions (both Van der Waals and repulsion effects appear - orange). Between the -NN- bridge and the subunits, there are two similar regions in **E-p-HPhAPN** (model *a*). The **Z-p-HPhAPN** (model *za*) contains only one wider region. A similar pattern is observed for **m-HPhAPN**. The pattern is changed in the case of the **o-HPhAPN** isomers. As the NBO and AIM earlier, the NCI method identifies the hydrogen bond between the hydrogen atom of the -OH group and the nitrogen N atom (o-HPhAPN (*b*, *i* and *zf* models). NCI also identifies repulsive forces in the ring of -O-H...N-N-C-C- atoms, which is consistent with the predictions of the AIM calculation in the case of the **o-HPhAPN**. A critical point of the (3,+1) type was detected in this ring.

Table 3. Second order perturbation energies $E^{(2)}$ (kcal·mol^{-1}) of donor-acceptor interactions between lone pairs of nitrogen atoms and antibonding C-C, C-N, O-H orbitals.

Donor-acceptor interactions		**Ab**		**p-HPhAPN**		**o-HPhAPN**	
		E-	Z-	E-	Z-	E-	
				a	*za*	*b*	*i*
LP(N_1)	C-C	9.9	11.1	11.0	11.8	10.1	10.8
	C-N	0.5	13.7	0.6	11.8	0	0.6
	O-H	0.0	0.0	0.0	0.0	0.0	0.0
LP(N'_1)	C-C	9.9	11.1	9.3	28.4	8.3	35.2
	C-N	0.5	13.7	0.0	11.1	1.3	47.8
	O-H	0.0	0.0	0.0	0.0	32.3	0.0
Total	C-C	19.8	22.2	20.3	40.2	18.4	46.0
	C-N	1.0	27.4	0.6	22.9	1.3	48.4
	O-H	0.0	0.0	0.0	0.0	32.3	0.0

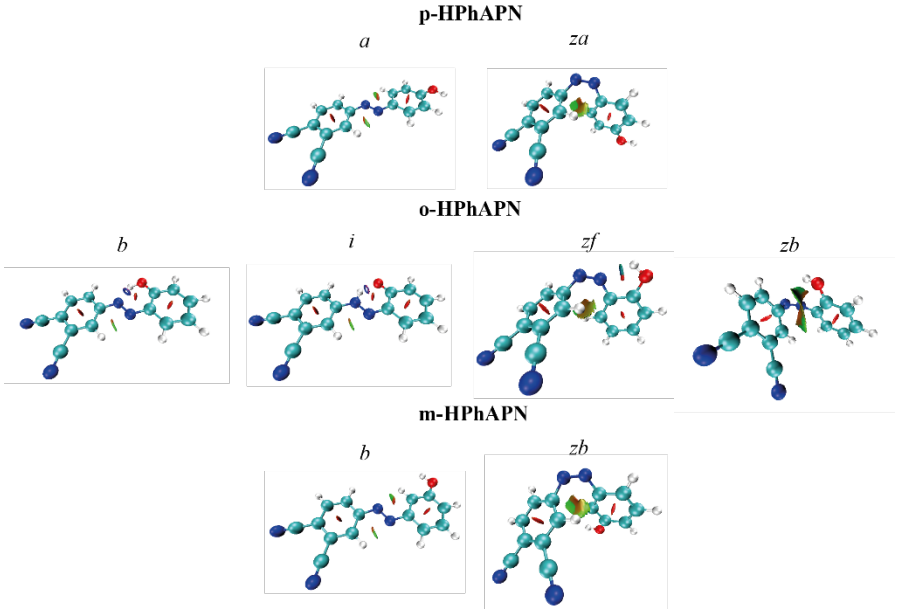

Figure 4. Spatial visualization of noncovalent interactions in the **HPhAPN** isomers**.** Noncovalent interactions are distinguished by the three different colors; blue color represents the hydrogen bonding while green – Van der Waals interactions and red represent the repulsive forces between atoms.

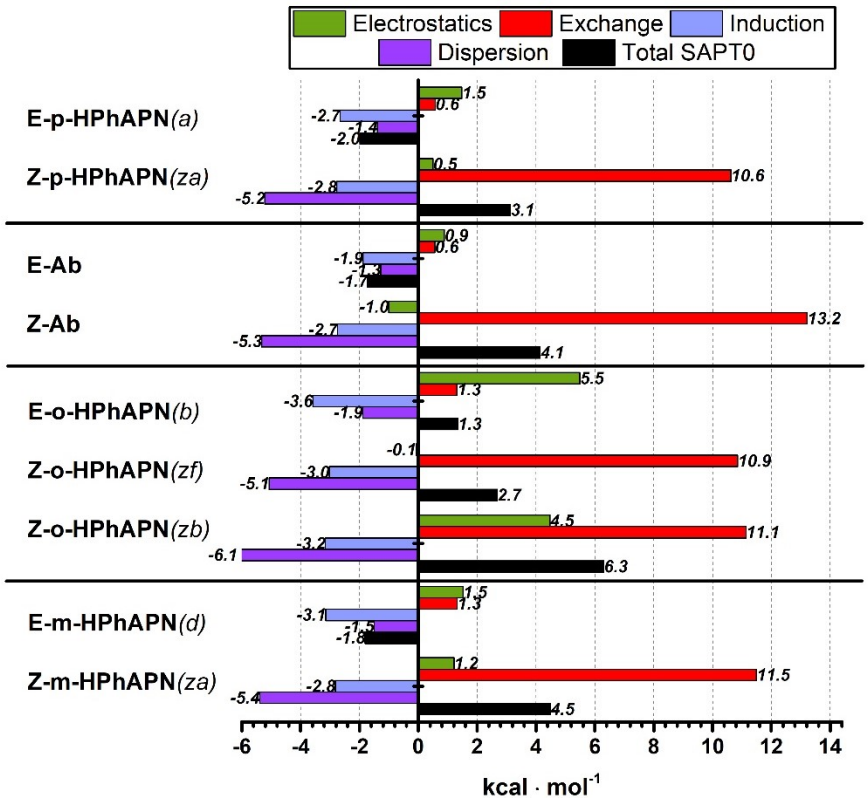

Figure 5. Results of the F/I-SAPT0 modeling for different E- and Z- derivatives of **Ab**.

F/I-SAPT0

Quantification of weak interactions is possible by F/I-SAPT0. This approach allows us to separate from each other both repulsive exchange (E_{exch}) and electrostatic (E_{el}) components in the total noncovalent energy E_{SAPT0}, and distinguish from each other different Van der Waals forces (E_{ind}, E_{disp}). The results of these calculations are listed in Figure 5. The F/I-SAPT0 extension allows the calculation of different SAPT energy terms between components within the embedding field of a third body, which allows to calculate the energy between functional groups/fragments within a single molecule using this method. The system HO-Ph-NN-Ph-2CN is divided into three subsystems: **A**(-Ph-OH) and

B(-Ph-2CN) the strength of the interaction of which we want to assess, as well as the link **C**(-NN-).

The F/I-SAPT0 method shows the stabilizing effect of induction and dispersion forces and the destabilizing role of the electrostatic and exchange component in all the structures studied. Total SAPT0 characterizes the summary effect of all the above types of interactions. Negative values indicate stabilization and positive values indicate destabilization.

Thus, E-structures are preferable for realization than the Z- structures in terms of F/I-SAPT0. This circumstance is explained by a sharp increase in the exchange of energy upon the transition to Z- structures. The stabilizing contribution of the other components increases in the Z-isomers, but this increase is much lower than that observed for E_{exch} energy. With an increase in the distances between the phenyl rings (distances $r_e(C_2 \cdots C_2')$ or distances between centers of phenyl rings) in a series of molecules **Z-m-HPhAPN→Z-Ab→Z-p-HPhAPN→Z-o-HPhAPN**, the energy ESAPT0 decreases.

Notably, the stabilizing contribution of ESAPT0 increases in the row of E-isomers of **o-HPhAPN→Ab→ m-HPhAPN→p-HPhAPN**, while only in the case of **E-o-HPhAPN** the ESAPT0 energy > 0 kcal·mol^{-1}. This is primarily due to an increase in the electrostatic repulsion energy between the **E-o-HPhAPN** subunits due to the closer location of the –OH group to PN in comparison with **E-m-HPhAPN** and **E-p-HPhAPN**. At the same time, in the case of Z-isomers, the ESAPT0 energy assumes the lowest value exactly in the case of **o-HPhAPN**.

Molecular vibrations and IR spectrum

The **E-Ab** molecule belongs to the C_{2h} point group and has 66 vibrational modes: $\Gamma_{vib} = 23A_g + 11A_u + 10B_g + 22B_u$. For **Z-Ab**, fundamental vibrations have the following distribution in the symmetry classes belonging to the C_2 point group: $\Gamma_{vib} = 34A + 32B$. Assignments of all vibration bands in **E-Ab**, **Z-Ab**, **p-HPhAPN** are presented in Tables 4 and 5, S2-S3. The performed analysis is in good agreement with the characterization described in the article.[44] Majority of normal modes are extended over entire molecule. According to the PED, most of the vibrations are comprised of displacements along several internal coordinates, which complicates the frequency assignment, especially in the case of Z-isomer. Majority of vibrations correspond to normal modes of benzene (Table S2). The seven low-energy vibrations do not relate to recognizable phenyl modes and may be considered as ring-ring modes in a similar way to the presented consideration of biphenyl.[46] For **Ab**, these vibrations can be described as internal rotation of phenyl moieties, in-plane and out-of-plane scissoring modes, two pairs of in-plane and out-of-plane shearing modes.

The IR spectra of E- and Z-isomers of **Ab** have some differences. The main difference, which is well determined experimentally,[44] concerns the strong bands in the region 690-800 cm^{-1}. For **E-Ab** the modes ω_{18} and ω_{21} (693 and 790 cm^{-1}) originates from out-of-plane bending of C-H and torsional motion of phenyl rings. In the case of **Z-Ab** the corresponding modes have lower IR intensities. However, there are two other intensive bands (715 and 776 cm^{-1}) in the spectrum of **Z-Ab**, corresponding to modes ω_{12} and ω_{20} that change strongly upon transition **E-Ab→Z-Ab**. They result essentially from the out of plane motions. Thereby upon **E-Ab→Z-Ab**, there is a decrease in the difference between the two strong bands (693 and 790, 715 and 776 cm^{-1}, respectively) (Figure 6). Thus, two intense peaks in the region 680-790 cm^{-1} are located more closely in the experimental IR spectrum of the **Z-Ab** compared to the **E-Ab** spectrum. It is also worth noting the appearance of medium bands at 1648, 1605, 934 cm^{-1}, corresponding to ω_{56}, ω_{52}, ω_{26}, which are IR inactive for the C_{2h} point group. It is worth pointing out that frequency of ω_{52} corresponding to NN stretching (with contribution of ~65%) increases by 50 cm^{-1} upon isomerization. Due to a decrease in IR intensity of ω_{39}, ω_{43}, ω_{46}, medium bands in the range from 1150 to 1400 cm^{-1} almost disappear in the spectrum of Z-isomer. The greatest differences in frequencies upon isomerisation are characteristic of modes with a significant contribution of azo bridge motions (Table S2). It should be noted that positions of bands in B3LYP/6-31G++G** simulated IR spectra of **E-Ab** and **Z-Ab** are in good agreement with appropriate values from experimental spectra[44] of azobenzenes isolated in an Ar matrix at 15 K (correlation between relevant bands of the experimental and model spectra is close to linear, Figure S4, Table S2).

Assignment of vibrational modes in **p-HPhAPN** is presented in Tables 5 and S3. Positions of bands in the simulated IR spectrum are in good agreement with appropriate values from the experimental spectrum in a solid phase (Figures 7 and S5). Correlation between relevant bands of the experimental and model spectra is close to linear: scaling coefficient is 0.969 (Figure S5). Upon the addition of cyano and hydroxy groups to different positions of **Ab** core, IR spectrum changes significantly (Figure 7). In these cases, most of the bands in the IR spectra have a strongly pronounced mixed character. The bands at 1184 and 1309 cm^{-1} can be assigned to motions of hydroxyl group (δ(O-H) and ν(O-C), respectively) in combination with CCH in-plane bending and CC stretching. For the normal modes ω_{46}=1162 and ω_{61}=1544 cm^{-1} with strong IR absorptions, there is predominant contribution of CCH in-plane bending coordinates. The medium bands in the range 1300-1500 cm^{-1} correspond to the CC stretching vibrations. Stretching of CC bonds in the -Ph-OH moiety determines the appearance of a strong band at 1657 cm^{-1}. Stretching vibrations of C≡N and C-H bonds occurs in the region near 2350 cm^{-1} and 3200 cm^{-1}, respectively.

Noticeable changes in the IR spectrum also occur when the position of the -OH group is changed (Figure 7). Upon **p-HPhAPN→m-HPhAPN** the infrared intensities of vibrations $\omega_{46,53,59\text{-}61,65}/\omega_{58}$ decreases/increases, which leads to changes in peak shapes at ~1160, ~1310 cm^{-1} and in the region 1450-1660 cm^{-1}. The proximity of the -OH group to nitrogen atoms and the corresponding formation of a hydrogen bond N···H leads to a strong shift of the ν(O-H) band from 3819 for **p-HPhAPN** to 3207 cm^{-1} for **o-HPhAPN**. In case of spectrum of **o-HPhAPN**, the bands 1468 and 1412 cm^{-1} of high intensities assigned to NN stretching and OH-in-plane bending.

The main differences between the spectra of **E-p-HPhAPN** and **Z-p-HPhAPN** is observed in the region of 1500-1700 cm^{-1} (Figure 6). First, this is due to a significant change in frequency by 61 cm^{-1} and an increase in the IR intensity of the NN stretching vibration ω_{60}, similarly as in the case of unsubstituted azobenzenes. Changes in the IR intensities of the corresponding vibrational modes upon E-→Z- is also found, which, together with the first factor, leads to the appearance of a strong peak at 1586 cm^{-1} in the spectrum of **Z-p-HPhAPN**.

Table 4. Descriptions[a] of several[b] vibrational modes for **E-Ab** and **Z-Ab**.

i	E-Ab				Z-Ab			
	sym	ω_i [c]	$I_{IR\,i}$ [d]	Descriptions [a]	sym	ω_i [c]	$I_{IR\,i}$ [d]	Descriptions [a]
1	A_u	21.4	0.1	rot(Ph);	A	45.2	0.0	rot(Ph); δ(N'$_1$N$_1$C$_2$); δ(N$_1$C$_2$C);
2	A_u	62.8	1.5	π scissoring;	A	69.3	0.4	π scissoring
3	B_u	85.1	2.1	δ scissoring;	B	287.1	5.8	δ(N$_1$C$_2$C); δ(N'$_1$N$_1$C$_2$); τ(CCCN)
4	B_g	111.0	0.0	π shearing;	B	44.3	1.4	rot(Ph); δ(N$_1$C$_2$C);
5	A_g	223.5	0.0	δ shearing;	A	272.6	0.4	δ(N'$_1$N$_1$C$_2$); δ(N$_1$C$_2$C); τ(Ph);
6	B_g	260.9	0.0	π shearing;	B	155.9	2.8	τ(CCCN); δ(N'$_1$N$_1$C$_2$);
7	A_g	306.8	0.0	δ shearing;	A	172.6	0.2	τ(CNNC); δ(N$_1$C$_2$C);
12	B_u	529.0	26.2	δ(N'$_1$N$_1$C$_2$); δ(N$_1$C$_2$C); δ(CCC);	B	715.0	93.0	π(C-H): π(C$_5$-H$_5$), π(C$_4$-H$_4$), π(C$_6$-H$_6$); δ(N'$_1$N$_1$C$_2$);
18	A_u	693.4	75.6	τ(Ph); π(C-H);	A	703.0	21.9	τ(Ph); π(C-H): π(C$_6$-H$_6$), π(C$_4$-H$_4$); ν(N$_1$-C$_2$); δ(CCC); ν(C-C);
20	B_g	772.8	0.0	π(C-H); π(N$_1$-C$_2$);	B	776.0	52.8	π(C-H): π(C$_5$-H$_5$); ν(N$_1$-C$_2$); δ(CCC); π(N$_1$-C$_2$); ν(C-C);
21	A_u	789.7	86.9	π(C-H); π(N$_1$-C$_2$);	A	787.5	15.7	π(C-H): π(C$_5$-H$_5$); π(N$_1$-C$_2$); ν(N$_1$-C$_2$);
26	B_g	942.8	0.0	π(C-H): π(C$_7$-H$_7$), π(C$_5$-H$_5$), π(C$_3$-H$_3$); τ(Ph)	B	934.2	21.0	π(C-H): π(C$_3$-H$_3$), π(C$_3$-H$_7$), π(C$_5$-H$_5$); π(N$_1$-C$_2$); δ(N'$_1$N$_1$C$_2$);
39	B_u	1176.9	29.6	δ(C-H): δ(C$_3$-H$_3$), δ(C$_4$-H$_4$), δ(C$_7$-H$_7$); ν(C-C); ν(N$_1$-C$_2$);	B	1173.5	1.9	ν(N$_1$-C$_2$); δ(C-H): δ(C$_3$-H$_3$); ν(C-C);
43	B_u	1258.8	23.9	ν(N$_1$-C$_2$); ν(C-C); δ(C-H): δ(C$_4$-H);	B	1202.4	0.2	δ(C-H): δ(C$_4$-H$_4$), δ(C$_6$-H$_6$); ν(C-C): ν(C$_3$-C$_4$); ν(N$_1$-C$_2$);
46	B_u	1363.0	8.8	ν(C-C): ν(C$_3$-C$_4$), ν(C$_5$-C$_6$), ν(C$_2$-C$_7$), ν(C$_4$-C$_5$), ν(C$_2$-C$_3$), ν(C$_6$-C$_7$); δ(C-H);	B	1354.4	0.7	ν(C-C): ν(C$_6$-C$_7$), ν(C$_3$-C$_4$), ν(C$_4$-C$_5$); δ(C-H): δ(C$_3$-H$_3$), δ(C$_7$-H$_7$), δ(C$_5$-H$_5$);
52	A_g	1557.2	0.0	ν(N$_1$-N'$_1$); ν(C-C); δ(C-H);	A	1605.0	25.3	ν(N$_1$-N'$_1$); ν(C-C);
56	A_g	1649.0	0.0	ν(C-C): ν(C$_6$-C$_7$), ν(C$_3$-C$_4$); δ(C-H); ν(N$_1$-N'$_1$);	A	1648.6	12.9	ν(C-C): ν(C$_6$-C$_7$), ν(C$_3$-C$_4$); ν(N$_1$-N'$_1$); δ(C-H);

[a]Based on PED. Coordinates are listed if their contributions are greater than ~10%. Coordinates are presented in descending order of their contributions. The designation "*Coord-1*: *Coord-2*, *Coord-3*;" means that the displacement along coordinates *Coord-2* and *Coord-3* are a part of the general displacement *Coord-1*. Given that the molecules have the symmetries C_{2h} and C_2, the following pairs of atoms are symmetrically equivalent: N'$_1$ and N$_1$, C$_2$ and C'$_2$, C$_3$ and C'$_3$, C$_4$ and C'$_4$, C$_5$ and C'$_5$, C$_6$ and C'$_6$, C$_7$ and C'$_7$, *etc.*, therefore it is assumed in assignment that, for example, vibration ν(C$_2$-C$_3$) includes both vibration ν(C$_2$-C$_3$) and ν(C'$_2$-C'$_3$), *etc*. The following designations are used: ν(X-Y) – stretching of the X–Y bond; δ – in-plane bending; π – out-of-plane bending; τ – torsion; rot(Ph) – rotation of the phenyl fragment around an axis N-C; π scissoring - ring-ring out-of-plane scissoring (with analogy at [46]); δ scissoring – ring-ring in-plane scissoring (with analogy at [46]); π shearing – out-of-plane shearing (with analogy at [46]); δ shearing – in-plane shearing (with analogy at [46]).
[b]Assignments of all vibration bands in **E-Ab** and **Z-Ab** are presented in Table S2;
[c]ω_i – calculated frequencies (cm^{-1});
[d]$I_{IR\,i}$ – calculated IR-intensities (km·mol^{-1}).

Table 5. Descriptions[a] of several[b] vibrational modes for **E-p-HPhAPN**.

i	ω_i [c]	$I_{IR\,i}$ [d]	Descriptions[a]
46	1162.0	302.1	δ(C-H): δ(C'$_7$-H'$_7$); ν(N-C): ν(N'$_1$-C'$_2$), ν(N$_1$-C$_2$); ν(C-C);
53	1309.1	278.4	ν(O-C); ν(C-C); δ(C-H); ν(N-C): ν(N'$_1$-C'$_2$);
58	1472.7	37.7	ν(C-C): ν(C'$_6$-C'$_7$), ν(C'$_3$-C'$_4$); δ(C-H): δ(C'$_4$-H'$_4$), δ(C'$_6$-H'$_6$); ν(N$_1$-N'$_1$);
59	1509.6	88.4	ν(C-C): ν(C$_4$-C$_5$); δ(C-H);
60	1523.5	104.7	ν(N$_1$-N'$_1$); ν(C-C); δ(C-H);
61	1544.3	296.1	δ(C-H); ν(C-C); ν(N$_1$-N'$_1$);
65	1657.2	260.0	ν(C-C): ν(C'$_6$-C'$_7$), ν(C'$_3$-C'$_4$), ν(C'$_4$-C'$_5$), ν(C'$_2$-C'$_7$); δ(C-H)

[a]Based on PED. Coordinates are listed if their contributions are greater than ~10%. Coordinates are presented in descending order of their contributions. The designation "*Coord-1*: *Coord-2*, *Coord-3*;" means that the displacement along coordinates *Coord-2* and *Coord-3* are a part of the general displacement *Coord-1*. The following designations are used: ν(X-Y) – stretching of the X–Y bond; δ – in-plane bending.
[b]Assignments of all vibration bands in the **E-p-HPhAPN** are presented in Table S3;
[c]ω_i – calculated frequencies (cm^{-1});
[d]$I_{IR\,i}$ – calculated IR-intensities (km·mol^{-1}).

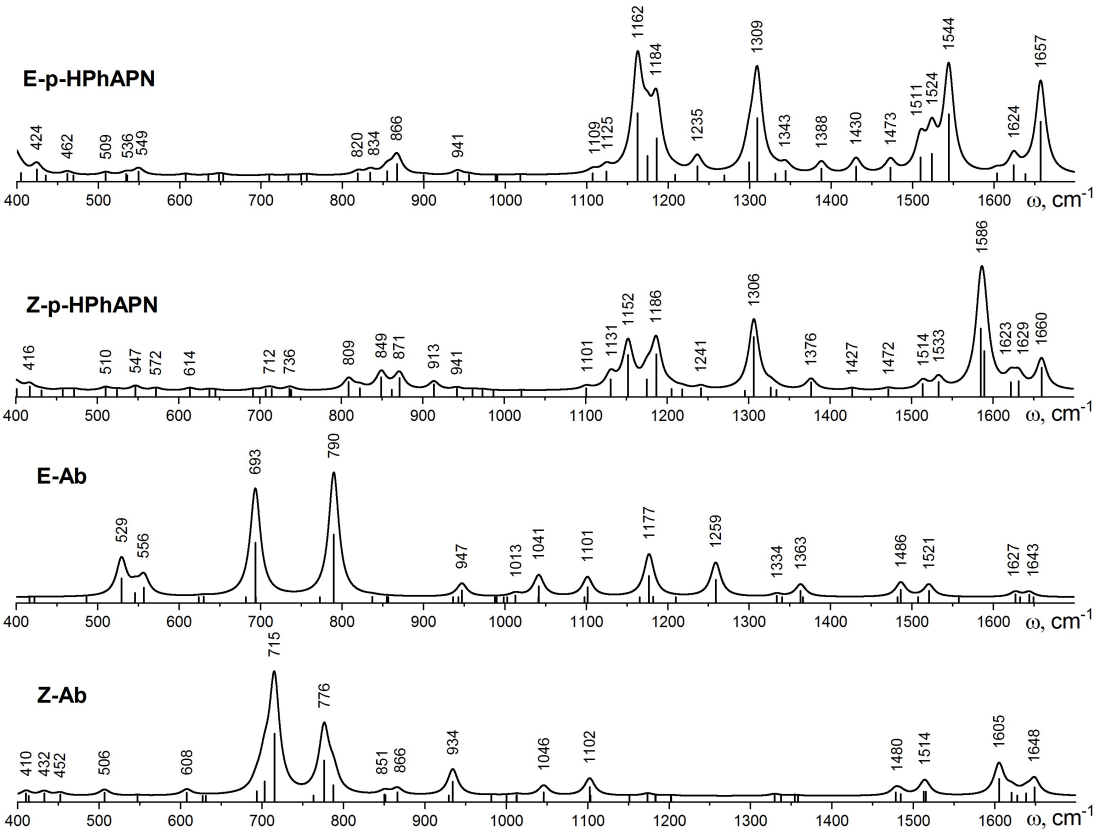

Figure 6. Simulated IR spectra for **E-pHPhAPN**, **Z-pHPhAPN**, **E-Ab**, **Z-Ab** in the 400–1700 cm^{-1} range. In order to simulate the shape of IR spectra, the individual bands were described by Lorentz curves with a half width of 15 cm^{-1}.

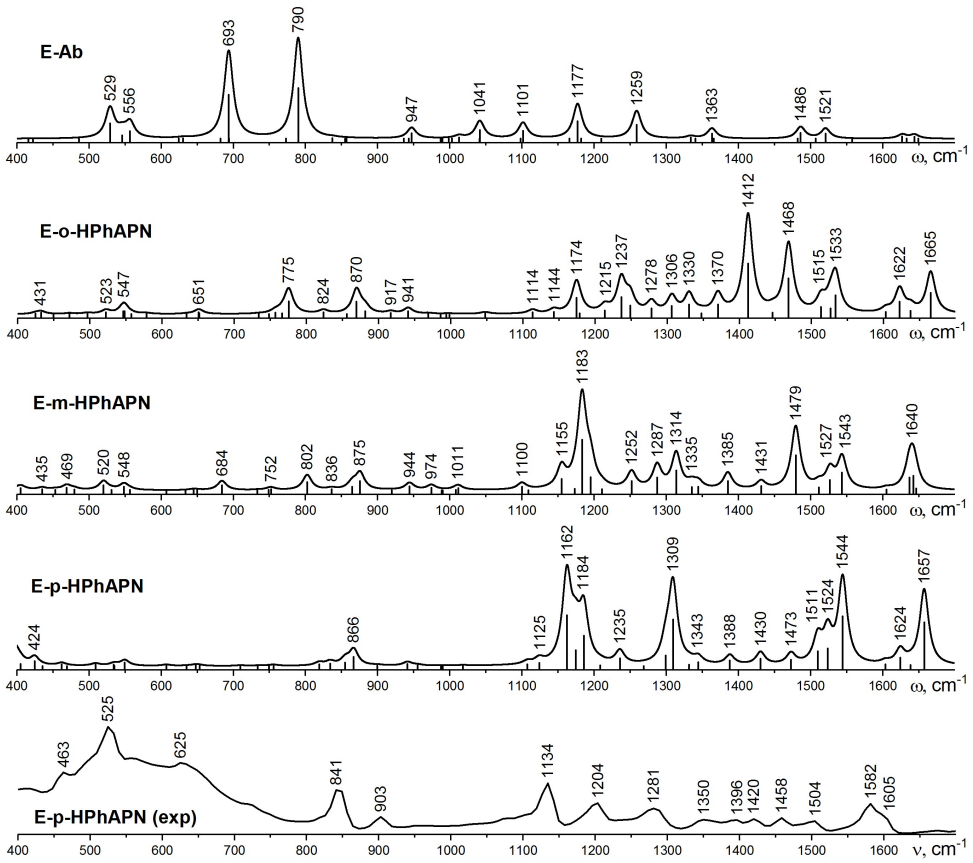

Figure 7. Simulated IR spectra for **E-Ab**, **E-o-HPhAPN**, **E-m-HPhAPN**, **E-p-HPhAPN** and experimental IR spectrum of **E-p-HPhAPN** in the 400–1700 cm^{-1} range.

Conclusions

The structure, isomeric and conformational diversity of azobenzenes substituted by hydroxyl and nitrile groups are studied by QC calculations. The functionalization of different phenyl rings by -CN and -OH substituents leads to some asymmetry in π-system delocalization: the interactions of -Ph-OH moiety with the azo bridge is manifested to a greater extent than in the case of -Ph-2CN fragment. The assignment of vibrational modes of **E-pHPhAPN** was carried out via potential energy distribution analysis among internal coordinates in comparison with appropriate analysis of initial **E-Ab**. The positions of the bands in the modeled B3LYP/6-31++G** spectrum of **E-pHPhAPN** are in good agreement with the appropriate values from the experimental spectrum. For azobenzenes, the transition from the E-isomer to the Z-isomer leads to strong changes in the geometric and electronic structure, which leads to noticeable changes in IR spectra.

Acknowledgements. The study was supported by the Russian Science Foundation (grant No. 22-73-00314). Experimental part was carried out using the resources of the Center for Shared Use of Scientific Equipment of the ISUCT (with the support of the Ministry of Science and Higher Education of Russia, grant No. 075-15-2021-671). The authors are grateful to Nina I. Giricheva for helpful suggestions and discussions.

Supplementary materials. The following are available online: Figure S1. Conformer and isomer models of **m-HPhAPN** and appropriate relative energies. Figure S2. Conformer and isomer models of **E-o-HPhAPN** and appropriate relative energies. Figure S3. Conformer and isomer models of **Z-o-HPhAPN** and appropriate relative energies. Figure S4. Correlation dependences between experimental and calculated wavenumbers of the absorption bands in the IR spectra of **E-Ab** and **Z-Ab**. Figure S5. Correlation dependences between experimental and calculated wavenumbers of the absorption bands in the IR spectra of **E-p-HPhAPN**. Table S1. Nucleus-independent chemical shifts indexes, Wiberg bond indexes and electron delocalization indexes calculated for **Ab**, **Ab-2OH**, **Ab-4CN**, **p-HPhAPN**, **m-HPhAPN**, **o-HPhAPN**. Table S2. Calculated frequencies, IR-intensities and vibrational modes descriptions for **E-Ab** and **Z-Ab**. Table S3. Calculated frequencies, IR-intensities and vibrational modes descriptions for **E-p-HPhAPN**. Additionally, optimized structures from QC calculations are given in Supplementary materials. Supplementary materials are available on the website *http://mhc-isuct.ru/*.

References

1. Fedele C., Ruoko T.-P., Kuntze K., Virkki M., Priimagi A. *Photochem. Photobiol. Sci.* **2022**, *21*, 1719–1734.
2. Giles L.W., Faul C.F.J., Tabor R.F. *Mater. Adv.* **2021**, *2*, 4152–4164.
3. Purkait M.K., Sinha M.K., Mondal P., Singh R. Photoresponsive Membranes. In: *Interface Science and Technology*, Vol. 25 (Purkait M.K., Sinha M.K., Mondal P., Singh R., Eds.), Elsevier, **2018**, Ch. 4, 115–144.
4. Natansohn A., Rochon P. *Chem. Rev.* **2002**, *102*, 4139–4176.
5. Manickasundaram S., Kannan P., Hassan Q.M.A., Palanisamy P.K. *J. Mater. Sci. Mater. Electron.* **2008**, *19*, 1045–1053.
6. Beharry A.A., Woolley G.A. *Chem. Soc. Rev.* **2011**, *40*, 4422–4437.
7. Mohr G.J., Müller H., Bussemer B., Stark A., Carofiglio T., Trupp S., Heuermann R., Henkel T., Escudero D., González L. *Anal. Bioanal. Chem.* **2008**, *392*, 1411–1418.
8. Shikhaliyev N.Q., Kuznetsov M.L., Maharramov A.M., Gurbanov A.V., Ahmadova N.E., Nenajdenko V.G., Mahmudov K.T., Pombeiro A.J.L. *CrystEngComm* **2019**, *21*, 5032–5038.
9. Tikhomirova T.V., Znoiko S.A., Shaposhnikov G.P. *Russ. J. Gen. Chem.* **2018**, *88*, 1164–1171.
10. Bouwstra J.A., Schouten A., Kroon J. *Acta Crystallogr.: Sect. C* **1983**, *39*, 1121–1123.
11. Brown C.J. *Acta Crystallogr.* **1966**, *21*, 146–152.
12. Harada J., Ogawa K., Tomoda S. *Acta Crystallogr.: Sect. B* **1997**, *53*, 662–672.
13. Ramesh Babu R., Kumaresan S., Vijayan N., Gunasekaran M., Gopalakrishnan R., Kannan P., Ramasamy P. *J. Cryst. Growth* **2003**, *256*, 387–392.
14. Zhang C.Z. *Acta Crystallogr.: Sect. E. Struct. Rep. Online* **2008**, *64*, o618.
15. Bushuyev O.S., Friščić T., Barrett C.J. *Cryst. Growth Des.* **2016**, *16*, 541–545.
16. Harada J., Ogawa K. *J. Am. Chem. Soc.* **2004**, *126*, 3539–3544.
17. Traetteberg M., Hillmo I., Hagen K. *J. Mol. Struct.* **1977**, *39*, 231–239.
18. Tsuji T., Takashima H., Takeuchi H., Egawa T., Konaka S. *J. Phys. Chem. A* **2001**, *105*, 9347–9353.
19. Mahmood A., Khan S.U.-D., Rana U.A. *J. Comput. Electron.* **2014**, *13*, 1033–1041.
20. Mahmood A., Tahir M.H., Irfan A., Al-Sehemi A.G., Al-Assiri M.S. *Comput. Theor. Chem.* **2015**, *1066*, 94–99.
21. *Gaussian 09, Revision D.01*. Frisch M.J., Trucks G.W., Schlegel H.B., Scuseria G.E., Robb M.A., Cheeseman J.R., Scalmani G., Barone V., Mennucci B., Petersson G.A., Nakatsuji H., Caricato M., Li X., Hratchian H.P., Izmaylov A.F., Bloino J., Zheng G., Sonnenberg J.L., Hada M., Ehara M., Toyota K., Fukuda R., Hasegawa J., Ishida M., Nakajima T., Honda Y., Kitao O., Nakai H., Vreven T., Montgomery J.A. Jr., Peralta J.E., Ogliaro F., Bearpark M., Heyd J.J., Brothers E., Kudin K.N., Staroverov V.N., Kobayashi R., Normand J., Raghavachari K., Rendell A., Burant J.C., Iyengar S.S., Tomasi J., Cossi M., Rega N., Millam J.M., Klene M., Knox J.E., Cross J.B., Bakken V., Adamo C., Jaramillo J., Gomperts R., Stratmann R.E., Yazyev O., Austin A.J., Cammi R., Pomelli C., Ochterski J.W., Martin R.L., Morokuma K., Zakrzewski V.G., Voth G.A., Salvador P., Dannenberg J.J., Dapprich S., Daniels A.D., Farkas O., Foresman J.B., Ortiz J.V., Cioslowski J., Fox D.J., Gaussian, Inc., Wallingford CT, **2009**.
22. Ditchfield R., Hehre W.J., Pople J.A. *J. Chem. Phys.* **1971**, *54*, 724–728.
23. Hehre W.J., Ditchfield K., Pople J.A. *J. Chem. Phys.* **1972**, *56*, 2257–2261.
24. Hariharan P.C., Pople J.A. *Theor. Chim. Acta* **1973**, *28*, 213–222.
25. Clark T., Chandrasekhar J., Spitznagel G.W., Schleyer P.V.R. *J. Comput. Chem.* **1983**, *4*, 294–301.
26. Feller D. *J. Comput. Chem.* **1996**, *17*, 1571–1586.
27. Schuchardt K.L., Didier B.T., Elsethagen T., Sun L., Gurumoorthi V., Chase J., Li J., Windus T.L. *J. Chem. Inf. Model.* **2007**, *47*, 1045–1052.
28. Pritchard B.P., Altarawy D., Didier B., Gibson T.D., Windus T.L. *J. Chem. Inf. Model.* **2019**, *59*, 4814–4820.

29. Glendening E.D., Badenhoop J.K., Reed A.E., Carpenter J.E., Bohmann J.A., Morales C.M., Weinhold F. *NBO Version 5.0*, Theoretical Chemistry Institute, University of Wisconsin, Madison, WI, **2001**.
30. Keith T.A. *AIMAll (Version 19.10.12)*, TK Gristmill Software, Overland Park KS, USA, **2019** (*aim.tkgristmill.com*).
31. Bushmarinov I.S., Lyssenko K.A., Antipin M.Y. *Russ. Chem. Rev.* **2009**, *78*, 283–302.
32. Jeziorski B., Moszynski R., Szalewicz K. *Chem. Rev.* **1994**, *94*, 1887–1930.
33. Parrish R.M., Parker T.M., Sherrill C.D. *J. Chem. Theory Comput.* **2014**, *10*, 4417–4431.
34. Parrish R.M., Gonthier J.F., Corminbœuf C., Sherrill C.D. *J. Chem. Phys.* **2015**, *143*, 051103.
35. Johnson E.R., Keinan S., Mori-Sánchez P., Contreras-García J., Cohen A.J., Yang W. *J. Am. Chem. Soc.* **2010**, *132*, 6498–6506.
36. Lu T., Chen F. *J. Comput. Chem.* **2012**, *33*, 580–592.
37. Smith D.G.A., Burns L.A., Simmonett A.C., Parrish R.M., Schieber M.C., Galvelis R., Kraus P., Kruse H., Di Remigio R., Alenaizan A., James A.M., Lehtola S., Misiewicz J.P., Scheurer M., Shaw R.A., Schriber J.B., Xie Y., Glick Z.L., Sirianni D.A., O'Brien J.S., Waldrop J.M., Kumar A., Hohenstein E.G., Pritchard B.P., Brooks B.R., Schaefer H.F., Sokolov A.Y., Patkowski K., DePrince A.E., Bozkaya U., King R.A., Evangelista F.A., Turney J.M., Crawford T.D., Sherrill C.D. *J. Chem. Phys.* **2020**, *152*, 184108.
38. Vishnevskiy Y.V., Zhabanov Y.A. *J. Phys. Conf. Ser.* **2015**, *633*, 012076.
39. Varsányi G. *Vibrational Spectra of Benzene Derivatives*, Academic Press, New York and London, **1969**,.
40. Varsányi G., Láng L. *Assignments for Vibrational Spectra of Seven Hundred Benzene Derivatives*, Wiley, **1974**,.
41. Gardner A.M., Wright T.G. *J. Chem. Phys.* **2011**, *135*, 114305.
42. Stepanić V., Baranović G., Smrečki V. *J. Mol. Struct.* **2001**, *569*, 89–109.
43. Gagliardi L., Orlandi G., Bernardi F., Cembran A., Garavelli M. *Theor. Chem. Acc.* **2004**, *111*, 363–372.
44. Duarte L., Fausto R., Reva I. *Phys. Chem. Chem. Phys.* **2014**, *16*, 16919–16930.
45. Armstrong D.R., Clarkson J., Smith W.E. *J. Phys. Chem.* **1995**, *99*, 17825–17831.
46. Katon J.E., Lippincott E.R. *Spectrochim. Acta* **1959**, *15*, 627–650.
47. Zhurko G.A. *Chemcraft - graphical software for visualization of quantum chemistry computations* (*https://www.chemcraftprog.com,* accessed Sept. 21, 2021).
48. Tikhomirova T.V., Gruzdeva O.M., Shaposhnikov G.P. *Russ. J. Gen. Chem.* **2015**, *85*, 2778–2785.
49. Fliegl H., Köhn A., Hättig C., Ahlrichs R. *J. Am. Chem. Soc.* **2003**, *125*, 9821–9827.
50. Hättig C., Hald K. *Phys. Chem. Chem. Phys.* **2002**, *4*, 2111–2118.
51. Briquet L., Vercauteren D.P., Perpète E.A., Jacquemin D. *Chem. Phys. Lett.* **2006**, *417*, 190–195.
52. Chen P.C., Chieh Y.C. *J. Mol. Struct. THEOCHEM* **2003**, *624*, 191–200.
53. Giricheva N.I., Lebedev I.S., Fedorov M.S., Bubnova K.E., Girichev G.V. *J. Struct. Chem.* **2021**, *62*, 1976–1987.
54. Tait K.M., Parkinson J.A., Gibson D.I., Richardson P.R., Ebenezer W.J., Hutchings M.G., Jones A.C. *Photochem. Photobiol. Sci.* **2007**, *6*, 1010–1018.
55. Girichev G.V., Tverdova N.V., Giricheva N.I., Savelyev D.S., Ol'shevskaya V.A., Ageeva T.A., Zaitsev A.V., Koifman O.I. *J. Mol. Struct.* **2019**, *1183*, 137–148.
56. Kurochkin I.Y., Pogonin A.E., Otlyotov A.A., Kiselev A.N., Krasnov A.V., Shlykov S.A., Girichev G.V. *J. Mol. Struct.* **2020**, *1221*, 128662.

Received 21.04.2023
Accepted 10.05.2023